Correlation between global polarization, angular momentum, and flow in heavy-ion collisions

Yu. B. Ivanov [1,2,3,*] and A. A. Soldatov[2]

[1]*Bogoliubov Laboratory for Theoretical Physics, Joint Institute for Nuclear Research, Dubna 141980, Russia*
[2]*National Research Nuclear University "MEPhI", Moscow 115409, Russia*
[3]*National Research Centre "Kurchatov Institute", Moscow 123182, Russia*

Possible correlations of the global polarization of Λ hyperons with angular momentum and transverse flow in the central region of colliding nuclei are studied based on a refined estimate of the global polarization. Simulations of Au + Au collisions at collision energies $\sqrt{s_{NN}} = 6$–40 GeV are performed within the model of the three-fluid dynamics. Within the crossover and first-order-phase-transition scenarios this refined estimate quite satisfactorily reproduces the experimental STAR data. Hadronic scenario fails at high collision energies, $\sqrt{s_{NN}} > 10$ GeV, and even predicts the opposite sign of the global polarization. It is found that the global polarization correlates with neither the angular momentum accumulated in the central region nor with directed and elliptic flow. At the same time we observed correlation between the angular momentum and directed flow in both their time and collision-energy dependence. These results suggest that, although initially the angular momentum is the driving force for the vortex generation, later the angular momentum and vortex motion become decorrelated in the midrapidity region. Then the midrapidity angular momentum is determined by the pattern of the directed flow and even becomes negative when the antiflow occurs. At the freeze-out stage, the dominant part of the participant angular momentum is accumulated in the fragmentation regions.

I. INTRODUCTION

Experimental observation of the global hyperon polarization in heavy-ion collisions by the STAR Collaboration at the BNL Relativistic Heavy Ion Collider (RHIC) [1–3] gave us the evidence for the creation of the most vortical fluid ever observed. Theoretical simulations within the hydrodynamic approaches [4–7] and transport models [8–12] based on thermal equilibration of the spin degrees of freedom [13–15] succeeded to describe the measured global hyperon polarization [1–3]. An alternative approach based on the axial vortical effect (AVE) [16–18] also reasonably reproduced the observed global polarization [19,20]. Although problems still persist, see recent review in Ref. [21], this gives us confidence that our current understanding of the heavy-ion dynamics and, in particular, the vortical motion is basically compatible with the observed polarization.

This phenomenon of the global polarization is usually related to the Barnett effect [22], i.e., magnetization by rotation, where a fraction of the orbital angular momentum associated with the body rotation is transformed into the spin angular momentum. In the Barnett effect the magnetization, i.e., spin alignment, is proportional to the angular momentum. On the contrary, the global hyperon polarization decreases with a rise in collision energy, i.e., with an increase of the total angular momentum [1–3]. This mismatch was explained by the global polarization being measured in the central region of

the colliding system (near the midrapidity), while the angular momentum is mostly accumulated in peripheral regions at the freeze-out stage [6,7,23,24]. Then the question arises: whether the global polarization in central region correlates with the angular momentum accumulated in this region? In the present paper we study this question.

We start with a more accurate estimate of the global polarization than that made in the previous paper [6]. Then we compare collision-energy dependence and time evolution of the global polarization and the angular momentum accumulated in the central region. We also compare the above quantities with those of directed and elliptic flow to test their possible correlation. The simulations are performed within the model of the three-fluid dynamics (3FD) [25] in the energy range of the Nuclotron based Ion Collider fAcility (NICA) in Dubna and the Beam Energy Scan (BES) program at RHIC.

II. POLARIZATION IN 3FD MODEL

High-energy heavy-ion collisions are characterized by a finite stopping power resulting in a counterstreaming regime of baryon-rich matter at an early stage of the collision. Within the 3FD [25] this nonequilibrium regime is modeled by two interpenetrating baryon-rich fluids initially associated with constituent nucleons of the projectile (p) and target (t) nuclei. Newly produced particles, predominantly populating the midrapidity region, are attributed to a fireball (f) fluid. Each of these fluids is governed by conventional hydrodynamic equations coupled by friction terms in the right-hand sides of the Euler equations. The physical input of the present

*yivanov@theor.jinr.ru

024916-1

3FD calculations is described in Ref. [26]. Three different equations of state (EoS's) were used in simulations. These are a purely hadronic EoS [27] and two versions of the EoS with the deconfinement transition [28], i.e., a first-order phase transition (1PT) and a crossover one.

The global polarization of hyperons was measured in the midrapidity region, i.e., at pseudorapidity $|\eta| < 1$ [1–3]. Similarly to that in Ref. [6], we associate the global midrapidity polarization with the polarization of Λ hyperons emitted from a central slab of the Au + Au colliding system

$$P_\Lambda \simeq \frac{\langle \varpi_{zx} \rangle}{2} \left(1 + \frac{2}{3} \frac{\langle E_\Lambda \rangle - m_\Lambda}{m_\Lambda} \right), \qquad (1)$$

where m_Λ is the mass of Λ hyperon, $\langle E_\Lambda \rangle$ is energy of the Λ hyperon averaged over the central slab, and $\langle \varpi_{zx} \rangle$ is the zx component of the thermal vorticity averaged over the central slab with the weight of the energy density ε:

$$\langle \varpi_{\mu\nu} \rangle(t) = \int_{\text{slab}} d^3 x \left[\varpi_{\mu\nu}^{\text{B}}(\mathbf{x}, t) \, \varepsilon_{\text{B}}(\mathbf{x}, t) \right.$$
$$\left. + \varpi_{\mu\nu}^{\text{f}}(\mathbf{x}, t) \, \varepsilon_{\text{f}}(\mathbf{x}, t) \right] / \langle \varepsilon \rangle(t), \qquad (2)$$

where

$$\varpi_{\mu\nu} = \tfrac{1}{2}(\partial_\nu \hat{\beta}_\mu - \partial_\mu \hat{\beta}_\nu), \qquad (3)$$

$\hat{\beta}_\mu = \hbar \beta_\mu$, $\beta_\mu = u_\nu/T$, u_μ is local four-velocity of a fluid, and T is local temperature. Here, B and f label quantities related to unified baryonic (p and t) fluid and the f fluid, respectively, and

$$\varepsilon \simeq \varepsilon_{\text{B}} + \varepsilon_{\text{f}}. \qquad (4)$$

In Eq. (1) all quantities are taken at the freeze-out instant. Expression (4) is a good approximation because of unification of the baryon-rich fluids and small relative (between baryon-rich and fireball fluids) velocities at the later stages of the collision [29].

The above equations need certain comments. Equation (1) (without averaging over the slab) was derived for a polarization vector averaged over the momentum direction of emitted hyperons [9]. In Ref. [6], where a narrow central slab was used, we neglected the longitudinal motion of the Λ hyperon in that slab and therefore approximated $\langle E_\Lambda \rangle$ by the mean midrapidity transverse mass, $\langle m_T^\Lambda \rangle_{\text{midrap.}}$. As we consider a wider slab in the present calculation (see discussion below), we compute $\langle E_\Lambda \rangle$ with an account of the longitudinal motion. We consider the proper-energy-density weighted vorticity (1) which allows us to suppress contributions of regions of low-density matter. It is appropriate because an abundant production of hyperons takes place in highly excited regions of the system.

A simplified version of the the freeze-out was used in Ref. [6]. The freeze-out instant was associated with time, when the energy density $\langle \varepsilon(t) \rangle$ averaged over the central slab reached the value of freeze-out energy density $\epsilon_{\text{frz}} = 0.4$ GeV/fm^3. This parameter is the same for all EoS's and all collision energies.

In actual calculations of observables a differential, i.e., cell-by-cell, freeze-out is implemented in the 3FD [30]. The
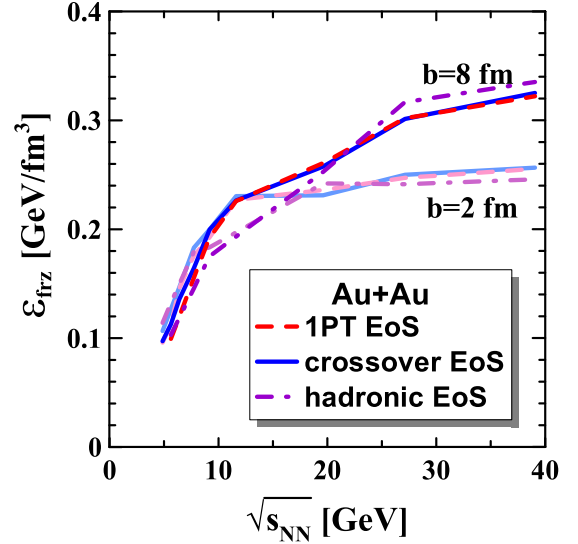

FIG. 1. Average actual freeze-out energy density versus collision energy $\sqrt{s_{NN}}$ in Au + Au collisions at impact parameters $b = 2$ and 8 fm calculated with different EoS's. Pale colors are used for $b = 2$ fm.

freeze-out procedure starts when the local energy density drops down to the freeze-out value ϵ_{frz}. The freeze-out criterion is checked in the analyzed cell and in eight cells surrounding this cell. If the freeze-out criterion is met in all cells and if the analyzed cell is adjacent to the vacuum (i.e., if at least one of the surrounding cells is "empty"[1]), then this considered cell is counted as frozen out. The latter condition prevents the formation of bubbles of frozen-out matter inside the dense matter still hydrodynamically evolving. This results in the actual energy density of frozen-out cell ε_{frz} being lower than ϵ_{frz}. Thus, ϵ_{frz} has a meaning of a "trigger" that indicates the possibility of freeze-out. The physical pattern behind this freeze-out resembles the process of expansion of a compressed and heated classical fluid into vacuum, mechanisms of which were studied both experimentally and theoretically, see discussion in Ref. [30]. The freeze-out is associated with evaporation from the surface of the expanding fluid.

The actual value ε_{frz} depends on the dynamics of expansion and consequently on the collision energy, EoS, and impact parameter (b). This actual freeze-out energy density, averaged over the frozen out system, is illustrated in Fig. 1.

We performed 3FD simulations of Au + Au collisions at fixed impact parameters $b = 8$ fm. This b was taken to roughly comply with the STAR centrality selection of 20–50 % [1]. Glauber simulations of Ref. [31] were used to relate the experimental centrality and the mean impact parameter. In the present calculation we also apply the global freeze-out in the central slab but at the actual freeze-out energy density as it is displayed in Fig. 1. Detailed discussion of ε_{frz} dependence versus collision energy is presented in Ref. [32]. In particular, it is responsible for the observed step-like behavior of mean transverse masses as a function of the collision energy [32].

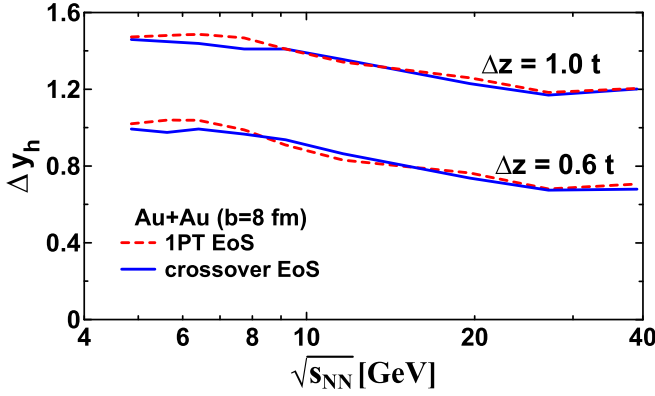[1]Frozen-out cells are removed from the hydrodynamical evolution.

FIG. 2. Rapidity width Δy_h ($|y_h| < \Delta y_h/2$) of the central slab at the freeze-out instant versus collision energy $\sqrt{s_{NN}}$ in Au + Au collisions at impact parameters $b = 8$ fm calculated with various EoS's for two different prescriptions for the spatial slab width, Eqs. (8) and (9).

FIG. 3. Global polarization of Λ hyperons in Au + Au collisions at $b = 8$ fm as function of collision energy $\sqrt{s_{NN}}$. Shaded bands for the crossover EoS and hadronic EoS indicate polarization sensitivity to choice of the central slab: the upper borders of these bands correspond to choice (8) and the lower borders to choice (9). STAR data on global Λ and $\bar{\Lambda}$ polarization [1] are also displayed.

The width of the central slab is chosen to model the experimental condition $|\eta| < 1$. In terms of the rapidity of Λ hyperons this approximately corresponds to $|y| < 0.7$. In this estimate we used mean transverse masses of Λ's measured in Ref. [33]. We calculate the rapidity based on hydrodynamical four-velocity u^μ:

$$y_h(z, t) = \frac{1}{2} \ln \frac{\langle u^0 + u^3 \rangle}{\langle u^0 - u^3 \rangle}, \tag{5}$$

where

$$\langle u^\mu \rangle(z, t) = \int dx^1 dx^2 \left[u_B^\mu \, \varepsilon_B + u_f^\mu \, \varepsilon_f \right] / \langle \varepsilon \rangle(z, t) \tag{6}$$

is the hydrodynamical four-velocity averaged over the xy plane with the weight of the proper energy density, cf. Eq. (2). We use subscript h to indicate that this is a hydrodynamical rapidity rather than a true one. We define the rapidity width of the central slab as follows:

$$\Delta y_h(t) = y_h(z_{\text{right}}, t) - y_h(z_{\text{left}}, t), \tag{7}$$

where z_{right} and z_{left} are the right and left borders of the slab, respectively. In order to approximately keep $\Delta y_h(t) \approx 1.4$, i.e., $|y_h| < \Delta y/2 \approx 0.7$, we take an expanding time central slab

$$z_{\text{right}}(t) = -z_{\text{left}}(t) = 0.5t. \tag{8}$$

We also did calculations with the central slab expanding with time as

$$z_{\text{right}}(t) = -z_{\text{left}}(t) = 0.3t \tag{9}$$

in order to simulate the standard STAR selection of the midrapidity region $|y| < 0.5$, i.e., $\Delta y_h(t) \approx 1$. Results of estimations of Δy_h at the freeze-out instant according to Eqs. (5)–(9) are shown in Fig. 2. As seen, the results are not perfect because Δy depends on $\sqrt{s_{NN}}$, but it approximately stays near desired values.

The above-described improvements of the polarization calculation increase the polarization as compared to that reported in Ref. [6]. The results of this refined estimate are presented
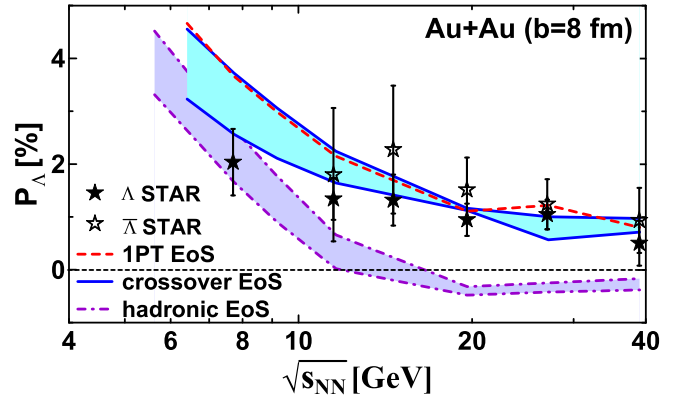
in Fig. 3. In order to get an impression of the effect of rapidity window Δy_h on the resulting polarization, we present calculations with two choices of the central slab: Eqs. (8) and (9). The polarization increases when the rapidity window expands because the polarization is higher at noncentral rapidities. While the global polarization predicted by the crossover and 1PT EoS's is very similar, this is not the case for the hadronic EoS. At high collision energies the hadronic-EoS results even in the negative polarization, which looks counterintuitive from the point of view of spin alignment along the angular momentum. This will be analyzed in more detail in the next section.

Overall agreement of the present estimate with the STAR data [1] on the Λ polarization is quite reasonable. The $\bar{\Lambda}$ polarization is very close to the Λ one, therefore we do not present it here. Note that the feed-down contribution to Λ polarization due to decays of higher mass hyperons is not taken into account in the present estimate. This feed-down results in about 10–15 % decrease of the resulting polarization, as demonstrated in Refs. [4,15,21,34].

III. CORRELATIONS BETWEEN POLARIZATION, ANGULAR MOMENTUM, AND FLOW

The method described above is not optimal for calculating the polarization, which can then be compared with experimental data. At the same time it provides a definite advantage for the study of the correlation between polarization and angular momentum. In this method we can compare the global polarization with the angular momentum accumulated in the same space region. The angular momentum accumulated in the slab region is defined as

$$J = \int_{\text{slab}} d^3x \sum_{\alpha=p,t,f} \left(z \, T_{10}^\alpha - x \, T_{30}^\alpha \right), \tag{10}$$

where $T_{\mu\nu}^\alpha$ is the energy-momentum tensor of the $\alpha(=p,t,f)$ fluid and has the conventional hydrodynamical form, z is the beam axis, (x, z) is the reaction plane of the colliding nuclei.
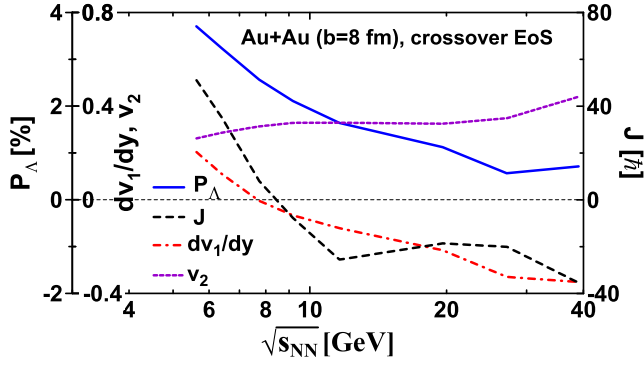
FIG. 4. Global polarization of Λ hyperons (P_Λ), angular momentum (J) accumulated in the "$|y_h| \lesssim 0.5$" slab, see Eq. (9), slope of the directed flow of matter (dv_1/dy) and elliptic flow (dv_2) at the freeze-out instant in Au + Au collisions at $b = 8$ fm as functions of the collision energy $\sqrt{s_{NN}}$. Calculations are performed with the crossover EoS.

In view of a further comparison of the polarization with slope of the directed flow in the center of colliding system, we consider a narrower "$|y_h| \lesssim 0.5$" slab, see Eq. (9), in this section. We also limit our further consideration to crossover and 1PT scenarios as the most relevant to the experimental data, see Fig. 3.

The directed flow of the matter is calculated as

$$v_1(y_h, t) = \left\langle \frac{u^1}{\sqrt{(u^1)^2 + (u^2)^2}} \right\rangle \quad (11)$$

in terms of the hydrodynamical four-velocities $u^\mu(x)$, $\langle \cdots \rangle$ means averaging over the xy plane with the weight of the proper energy density and summation over fluids similarly to Eq. (6). The corresponding rapidity y_h is defined by Eq. (5) in terms of the same hydrodynamical four-velocities. The slope of v_1 in the center of the colliding system, i.e., at "midrapidity" $y_h = 0$, is calculated as

$$\frac{dv_1(t)}{dy_h} = \frac{v_1(y_{\text{right}}, t) - v_1(y_{\text{left}}, t)}{y_{\text{right}}(t) - y_{\text{left}}(t)}, \quad (12)$$

where $y_{\text{right}}(t)$ and $y_{\text{left}}(t)$ are y_h rapidities at the right and left borders of the slab, respectively, cf. Eq. (7). Elliptic flow of the matter at "midrapidity" $y_h = 0$ is defined similarly:

$$v_2(t) = \left\langle \frac{(u^1)^2 - (u^2)^2}{(u^1)^2 + (u^2)^2} \right\rangle. \quad (13)$$

Here, the $\langle \cdots \rangle$ averaging is done over the $z = 0$ plane. The above-defined quantities at the freeze-out instant are presented in Figs. 4 (for the crossover EoS) and 5 (for the 1PT EoS) as functions of the collision energy.

Figures 4 and 5 demonstrate that the global polarization does not correlate with the angular momentum (J) accumulated in the central slab. This angular momentum first decreases with the collision energy rise and then flattens at higher energies. Moreover, the angular momentum becomes negative at higher collision energies while the global polarization remains positive. This behavior of the angular momentum in the central slab is completely different from that of the
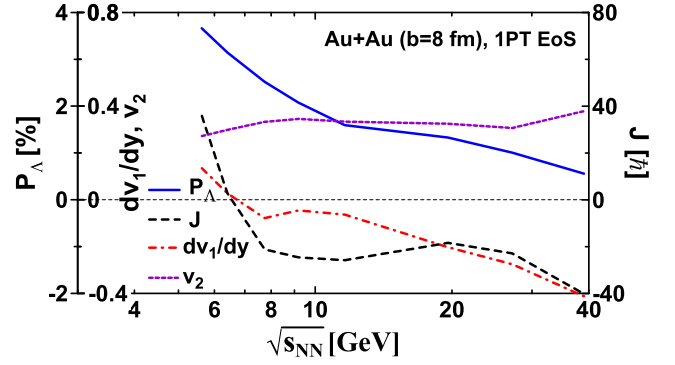

FIG. 5. The same as in Fig. 4 but for the 1PT EoS.

angular momentum accumulated in the whole participant region. The latter steadily increases with the collision energy rise [6,7]. Absence of correlation between the global polarization and the angular momentum was found already in Ref. [4]. However, there the authors considered the angular momentum accumulated in the whole participant region which steadily rises with the collision energy.

In fact, the absence of correlation between the global polarization and the angular momentum is not surprising. The polarization is intrinsically related to the vorticity while the rotation of the fluid can be vortex-free. In such vortex-free rotation the vorticity is present only in close vicinity of the axis of the rotation, if there is matter in this vicinity. Thus, the angular momentum can be arbitrarily large while the global polarization may be generated only in the narrow region around the rotation axis. Moreover, there could be local islands, where the matter vortically rotates in the opposite direction to the global rotation. Then the angular momentum and the global polarization can have opposite signs, as is the case in the Au + Au collisions at $b = 8$ fm, see Figs. 4 and 5. Such an island structure in the xz plane was observed in many simulations of nuclear collisions [8–10,23,24,35,36].

This island structure in the xz plane is illustrated in Fig. 6, where we present snapshots of the time evolution of the thermal zx vorticity (left column) and the proper energy density (right column) in the reaction plane in the semicentral ($b = 8$ fm) Au + Au collision at $\sqrt{s_{NN}} = 19.6$ GeV. In Figs. 4 and 5 we analyze the polarization and angular momentum accumulated in the central slab corresponding to the $|y_h| \lesssim 0.5$ condition. Borders of this central slab are indicated by dashed lines around the origin of the x axis in the left panels of Fig. 6. Quadrupole structure of vorticity field starts to form already at an early stage of the collision, i.e., at $t \lesssim 2$ fm/c, but the vortex, rotating along the total angular momentum of the system, still dominates in the central slab. At later stages the strong positive vorticity (i.e., corresponding to the sign of the total angular momentum of the system) is pushed out to target and projectile fragmentation regions, which suggests an increase in the polarization from the midrapidity to the fragmentation regions, as it was argued in Refs. [6,7]. While the polarization in the central slab is a matter of a delicate balance between vortices and antivortices, i.e., those rotating against the total angular momentum. The region of high
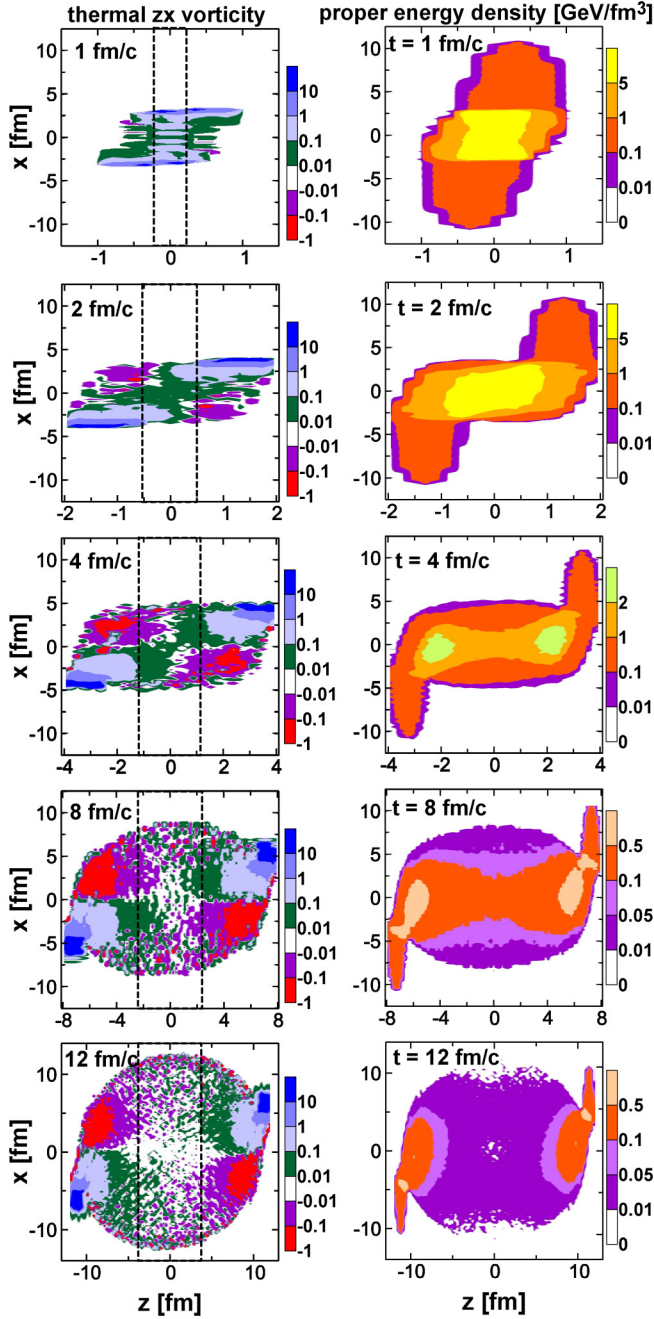
FIG. 6. The thermal zx vorticity (left column) and the proper energy density (right column) in the reaction plane at various time instants in the semicentral ($b = 8$ fm) Au + Au collision at $\sqrt{s_{NN}} = 19.6$ GeV. Calculations are done with the crossover EoS. z axis is the beam direction. Note the different scale along the z axis at different time instants. Dashed lines around the origin of the x axis in the left panels indicate borders of the central slab corresponding to the $|y_h| \lesssim 0.5$ condition.
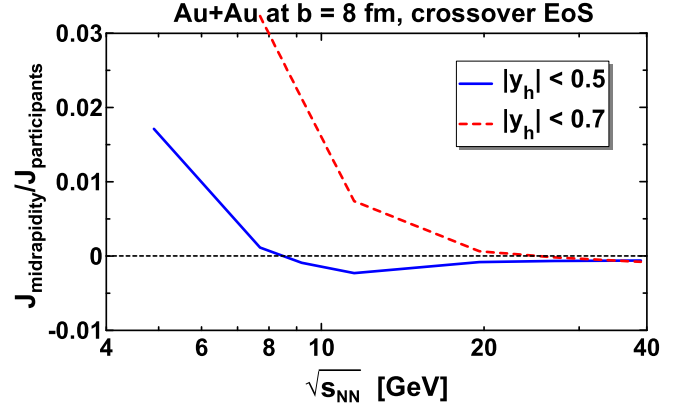

FIG. 7. Ratio of the angular momentum in the midrapidity region over the angular momentum accumulated by all participants at the freeze-out instant in semicentral ($b = 8$ fm) Au + Au collisions as function of $\sqrt{s_{NN}}$. Results are presented for two midrapidity regions (central slabs) corresponding to the $|y_h| \lesssim 0.5$ and $|y_h| \lesssim 0.7$ conditions. Calculations are done with the crossover EoS.

hadronic EoS changes this balance in such a way that the polarization becomes even slightly negative at high collision energies, see Fig. 4.

The pattern of the kinematic vorticity, i.e., that without extra factor $1/T$ in Eq. (3), is very similar to that of the thermal vorticity. Of course, neither the thermal vorticity nor the kinematic vorticity do not characterize the angular momentum, in particular, because of the possible vortex-free rotation mentioned above. However, they give us an impression of the direction of the rotation in the system. As seen from the vorticity field in the central slab, there is no obviously preferable direction of the matter rotation. Therefore, the angular momentum accumulated in the central slab is also a matter of a delicate balance between vortices, antivortexes, and possible vortex-free rotation of the matter that cannot be seen in Fig. 6. Moreover, $|J| \approx 20\hbar$ at $\sqrt{s_{NN}} = 19.6$ GeV in the central slab, see Figs. 4 and 5, whereas the total angular momentum accumulated in the participant region is $J_{\text{participants}} \approx 2 \times 10^4 \hbar$, see Refs. [6,7], i.e., three orders of magnitude higher than $|J|$.

Similar situation takes place at other collision energies, see Fig. 7. The value of $|J|$ at the freeze-out instant does not exceed a few percent of the total participant angular momentum in all considered energy ranges. As seen from Fig. 7, the midrapidity angular momentum rapidly decreases with collision energy rise and even becomes negative at high collision energies. The midrapidity angular momentum is larger in the wider ($|y_h| \lesssim 0.7$) midrapidity range than that in the narrower ($|y_h| \lesssim 0.5$) one. This once again indicates that the angular momentum is concentrated in fragmentation regions at the freeze-out instant. As this midrapidity angular momentum does not correlate with global polarization and hence with the vortical motion we can assume that it can be associated with a collective flow pattern in the midrapidity region.

Figures 4 and 5 also demonstrate collective flow. Scales of the slopes of the directed flow (dv_1/dy) and elliptic flow
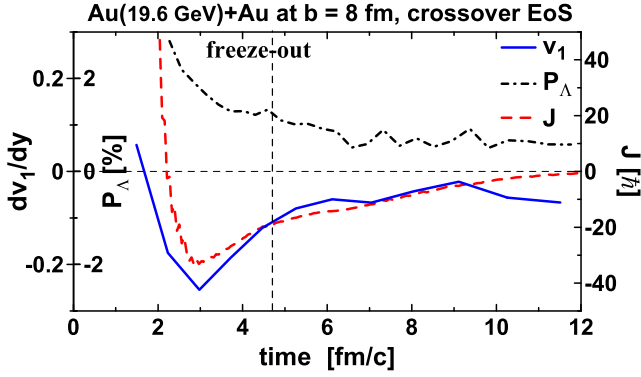
energy density is slightly inclined towards spectators. This enhances the contribution of the vortices in the global polarization because the hyperons are predominantly produced in highly excited regions. The delicate balance between vortices and antivortexes depends on the used EoS. Apparently, the

FIG. 8. Time evolution of the global polarization of Λ hyperons (P_Λ), angular momentum (J) accumulated in the "$|y_h| \lesssim 0.5$" slab, see Eq. (9), and slope of the directed flow of matter (dv_1/dy) in Au + Au collisions at $\sqrt{s_{NN}} = 19.6$ GeV and $b = 8$ fm. The vertical dashed line indicates the freeze-out instant. Calculations are performed with the crossover EoS.

(v_2) in Figs. 4 and 5 noticeably exceed those observed in the experiment. This is because the considered quantities characterize the medium rather than observed particles. The flow of observed particles is considerably smeared out by thermal spread and resonance decays [37,38]. The angular momentum characterizes the medium. Therefore, we compare it with the flow of the medium rather than specific particles.

As seen, the slope of the directed flow (dv_1/dy) does not correlate with the polarization but does correlate with the slab angular momentum. The slope and the angular momentum even simultaneously change their signs. This indicates that tilting the central fireball, which causes the antiflow [39,40], is accompanied by a change in its angular momentum. At the same time the elliptic flow (v_2) correlates with neither the polarization nor the angular momentum.

In order to check whether this flow–angular-momentum correlation in their $\sqrt{s_{NN}}$ dependence is accidental or not, we also consider their time dependence at various energies. Examples of such time dependence are presented in Figs. 8 and 9. The time dependence indicates that indeed there is a correlation between the v_1 slope and angular momentum, which is less spectacular at lower collision energies, see Fig. 9. Apparently, this is because the chosen width of the
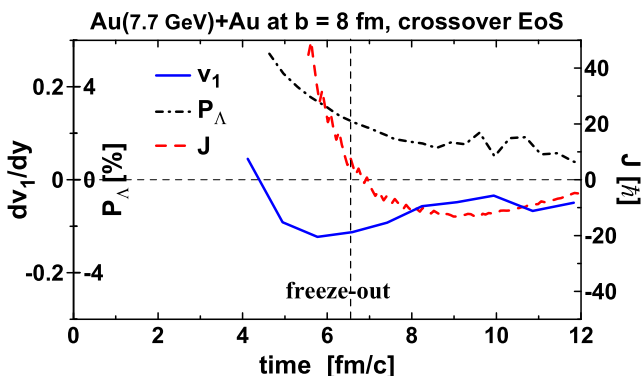
central region, $|y_h| \lesssim 0.5$, is too large at lower collision energies in view of comments below. A correlation between v_1 flow and polarization is also absent in their time dependence.

Note that the slope of the directed flow (dv_1/dy) in Figs. 8 and 9 at the freeze-out instant is slightly different from that presented in Fig. 4. In Figs. 8 and 9, the directed flow is calculated at the Lagrangian stage of the code [25] in terms of test particles and with smaller steps in y_h rapidity than in Eq. (12), while that in Fig. 4, see Eq. (12), is computed on a fixed grid (so-called Euler step of the scheme). The Lagrangian calculation is more accurate but more time consuming than the Euler one. Therefore, we performed this Lagrangian calculation with a larger time step than the Euler one. To accurately fix the freeze-out instant (as in Fig. 4), we need a finer time step.

IV. SUMMARY

Possible correlations of the global polarization of Λ hyperons with the angular momentum and transverse flow in the central region of colliding nuclei are studied based on a refined estimate of the global polarization within the 3FD model. In the present approach the global polarization is associated with the Λ polarization in the central region of colliding nuclei. Within the crossover and first-order-phase-transition scenarios this estimate quite satisfactorily reproduces the experimental STAR data [1], especially its collision-energy dependence. The purely hadronic scenario fails at high collision energies, $\sqrt{s_{NN}} > 10$ GeV, and even predicts the opposite sign of the global polarization.

It is found that the global polarization correlates with neither the angular momentum accumulated in the central region nor with directed and elliptic flow. Contrary to the polarization, the angular momentum accumulated in the central region even changes its sign at later stages of nuclear collisions at high collision energies. At the same time we detected a correlation between the angular momentum and directed flow. The midrapidity slope of the directed flow and the angular momentum even almost simultaneously change their signs.

The obtained results indicate that although initially the angular momentum is the driving force for the vortex generation, later the angular momentum and vortex motion become decorrelated in the midrapidity region. Then the midrapidity angular momentum is determined by the pattern of the directed flow and its value becomes less then a few percent of the angular momentum accumulated by participants and even becomes negative when the antiflow occurs. The dominant part of the participant angular momentum is accumulated in the fragmentation regions at the freeze-out stage.

FIG. 9. The same as in Fig. 8 but for $\sqrt{s_{NN}} = 7.7$ GeV.

[1] L. Adamczyk *et al.* (STAR Collaboration), Nature **548**, 62 (2017).

[2] J. Adam *et al.* (STAR Collaboration), Phys. Rev. C **98**, 014910 (2018).

[3] T. Niida (STAR Collaboration), Nucl. Phys. A **982**, 511 (2019).

[4] I. Karpenko and F. Becattini, Eur. Phys. J. C **77**, 213 (2017).

[5] Y. Xie, D. Wang, and L. P. Csernai, Phys. Rev. C **95**, 031901(R) (2017).

[6] Y. B. Ivanov, V. D. Toneev, and A. A. Soldatov, Phys. Rev. C **100**, 014908 (2019).

[7] Y. B. Ivanov, V. D. Toneev, and A. A. Soldatov, Phys. At. Nucl. **83**, 179 (2020).

[8] H. Li, L. G. Pang, Q. Wang, and X. L. Xia, Phys. Rev. C **96**, 054908 (2017).

[9] E. E. Kolomeitsev, V. D. Toneev, and V. Voronyuk, Phys. Rev. C **97**, 064902 (2018).

[10] O. Vitiuk, L. V. Bravina, and E. E. Zabrodin, Phys. Lett. B **803**, 135298 (2020).

[11] D. X. Wei, W. T. Deng, and X. G. Huang, Phys. Rev. C **99**, 014905 (2019).

[12] S. Shi, K. Li, and J. Liao, Phys. Lett. B **788**, 409 (2019).

[13] F. Becattini, V. Chandra, L. Del Zanna, and E. Grossi, Ann. Phys. (NY) **338**, 32 (2013).

[14] R.-h. Fang, L.-g. Pang, Q. Wang, and X.-n. Wang, Phys. Rev. C **94**, 024904 (2016).

[15] F. Becattini, I. Karpenko, M. A. Lisa, I. Upsal, and S. A. Voloshin, Phys. Rev. C **95**, 054902 (2017).

[16] A. Vilenkin, Phys. Rev. D **21**, 2260 (1980).

[17] J. H. Gao, Z. T. Liang, S. Pu, Q. Wang, and X. N. Wang, Phys. Rev. Lett. **109**, 232301 (2012).

[18] A. Sorin and O. Teryaev, Phys. Rev. C **95**, 011902(R) (2017).

[19] M. Baznat, K. Gudima, A. Sorin, and O. Teryaev, Phys. Rev. C **97**, 041902(R) (2018).

[20] Y. Sun and C. M. Ko, Phys. Rev. C **96**, 024906 (2017).

[21] F. Becattini and M. Lisa, Annu. Rev. Nucl. Part. Sci (2020), doi: 10.1146/annurev-nucl-021920-095245.

[22] S. J. Barnett, Phys. Rev. **6**, 239 (1915).

[23] Y. B. Ivanov and A. A. Soldatov, Phys. Rev. C **95**, 054915 (2017).

[24] Y. B. Ivanov and A. A. Soldatov, Phys. Rev. C **97**, 044915 (2018).

[25] Yu. B. Ivanov, V. N. Russkikh, and V. D. Toneev, Phys. Rev. C **73**, 044904 (2006).

[26] Yu. B. Ivanov, Phys. Rev. C **87**, 064904 (2013).

[27] V. M. Galitsky and I. N. Mishustin, Sov. J. Nucl. Phys. **29**, 181 (1979).

[28] A. S. Khvorostukhin, V. V. Skokov, K. Redlich, and V. D. Toneev, Eur. Phys. J. C **48**, 531 (2006).

[29] Y. B. Ivanov and A. A. Soldatov, Phys. Rev. C **98**, 014906 (2018); **101**, 024915 (2020).

[30] V. N. Russkikh and Yu. B. Ivanov, Phys. Rev. C **76**, 054907 (2007); Yu. B. Ivanov and V. N. Russkikh, Phys. At. Nucl. **72**, 1238 (2009).

[31] B. I. Abelev *et al.* (STAR Collaboration), Phys. Rev. C **79**, 034909 (2009).

[32] Y. B. Ivanov, Phys. Rev. C **89**, 024903 (2014).

[33] J. Adam *et al.* (STAR Collaboration), arXiv:1906.03732.

[34] F. Becattini, G. Cao, and E. Speranza, Eur. Phys. J. C **79**, 741 (2019).

[35] F. Becattini *et al.*, Eur. Phys. J. C **75**, 406 (2015); **78**, 354(E) (2018).

[36] Y. Jiang, Z.-W. Lin, and J. Liao, Phys. Rev. C **94**, 044910 (2016); **95**, 049904(E) (2017).

[37] Y. B. Ivanov and A. A. Soldatov, Phys. Rev. C **91**, 024914 (2015); Y. B. Ivanov, Phys. Lett. B **723**, 475 (2013).

[38] V. P. Konchakovski, W. Cassing, Y. B. Ivanov, and V. D. Toneev, Phys. Rev. C **90**, 014903 (2014); Y. B. Ivanov and A. A. Soldatov, *ibid.* **91**, 024915 (2015); Eur. Phys. J. A **52**, 10 (2016).

[39] J. Brachmann, S. Soff, A. Dumitru, H. Stöcker, J. A. Maruhn, W. Greiner, L. V. Bravina, and D. H. Rischke, Phys. Rev. C **61**, 024909 (2000).

[40] L. Csernai and D. Rohrich, Phys. Lett. B **458**, 454 (1999).

[41] http://ckp.nrcki.ru/.